IJCFD, 1999, Vol. 11, pp. 193–210
Reprints available directly from the publisher
Photocopying permitted by license only

Freezing of Water in a Differentially Heated Cubic Cavity

T. A. KOWALEWSKI [a] and M. REBOW [b]

[a] *IPPT PAN, Center of Mechanics and Information Technology, Polish Academy of Sciences, Swietokrzyska 21, PL 00-049 Warszawa, Poland;*
[b] *Warsaw University of Technology, Institute of Heat Engineering, ITC-PW, Nowowiejska 25, PL 00-665 Warszawa, Poland*

(Received in final form 30 August 1998)

An experimental and numerical study has been made of transient natural convection of water freezing in a cube-shaped cavity. The effect of the heat transfer through the side walls is studied in two configurations: with the cavity surrounded by air and with the cavity immersed in an external water bath of constant temperature. The experimental data for the velocity and temperature fields are obtained using liquid crystal tracers. The transient development of the ice/water interface is measured. The collected data are used as an experimental benchmark and compared with numerical results obtained from a finite-difference code with boundary fitted grid generation. The computational model has been adopted to simulate as closely as possible the physical experiment. Hence, fully variable fluid properties are implemented in the code, and, to improve modelling of the thermal boundary conditions, the energy equation is also solved inside the bounding walls. Although the general behaviour of the calculated ice front and its volume matches observations, several details of the flow structure do not. Observed discrepancies between experimental and numerical results indicate the necessity of verifying and improving the usual assumptions for modelling ice formation.

Keywords: Natural convection, freezing, phase change, experimental benchmark, water density anomaly, liquid crystals, particle image velocimetry and thermometry, boundary fitted grid, finite differences vorticity-vector potential method

1. INTRODUCTION

Fluid flow and thermal effects during melting and solidification are of great interest in a number of manufacturing processes, where a solid material is formed by the freezing of a liquid. The characteristic is that of a moving interface which separates two phases with different physical properties. Temperature differences in the melt give rise to buoyancy forces that produce significant convective flow. This flow modifies the heat transfer and the interface itself. It appears that there is a close relationship between the structure of the solid formed and the convective flow in the melt (Gau *et al.*, 1983). The analysis of the underlying process is important for casting, welding, soldering, processing of alloys or crystal growth. Proper modelling of these problems becomes necessary for

controlling fundamental parameters of the technological applications.

Due to the problem complexity direct application of numerical methods to the engineering problems is not a trivial task (Ramachandran, 1982; Viswanath *et al.*, 1993). Errors appearing due to limited accuracy of different numerical methodologies (Banaszek *et al.*, 1998), and due to inevitable simplifications introduced in the models, are usually difficult to predict *a priori*. Hence, the experimental verification of numerical models has special importance for phase change problems. To avoid geometrical complications and uncertainty of the thermophysical properties, often a simple model of water freezing in a differentially heated cavity is used for code testing purposes (Yeoh *et al.*, 1990). However, the available comparisons with experiment appear to be insufficient. This is, perhaps, due to the fact that most of the accessible experimental data on freezing are limited to general observations of the phase change front and point measurements of the flow velocity and temperature.

The main aim of the present investigation is to create an experimental benchmark for the problem of natural convection in freezing water. It consists of transient data on the interface position, and the temperature and velocity fields – gained by new full field experimental methods (Kowalewski *et al.*, 1997). The experimental results gained are compared with numerical simulations performed using the modified 3-D finite difference code FREEZE3D (Yeoh, 1993). The well known phenomena of the highly non-linear relationship between density and temperature in the vicinity of the freezing point (Robillard *et al.*, 1981; Lin *et al.*, 1987) puts an additional challenging complexion on the numerical simulation of the problem.

2. FORMULATION OF THE PROBLEM

We consider convective flow in a box filled with a viscous heat conducting liquid, which in this case is distilled water. The fluid density, viscosity, thermal conductivity and heat capacity are assumed to be temperature dependent. The flow takes place in a container with an aspect ratio of one, its two opposite vertical walls are assumed isothermal (Fig. 1). One of the vertical walls is held at temperature $T_c = -10°C$. It is below the freezing temperature of the liquid $T_r = 0°C$, hence the solid forms there. The opposite vertical wall is held at temperature $T_h = 10°C$. The other four walls of low thermal conductivity allow the entry of heat from the external fluid which surrounds the cavity. To investigate the effects of non-ideal thermal boundary conditions at these "side" walls two cases are considered. In the first the cavity is surrounded by a laminar air stream at temperature $T_{ext} = 25°C$, in the second case the water bath of constant temperature $T_{ext} = T_h$ surrounds the cavity. The temperature field at the inner surfaces of the walls adjusts itself depending on both the flow inside the box and the heat flux through and along the walls.

For transient processes uncertainty of the initial conditions may create difficulties in matching experimental and numerical results. Hence, two

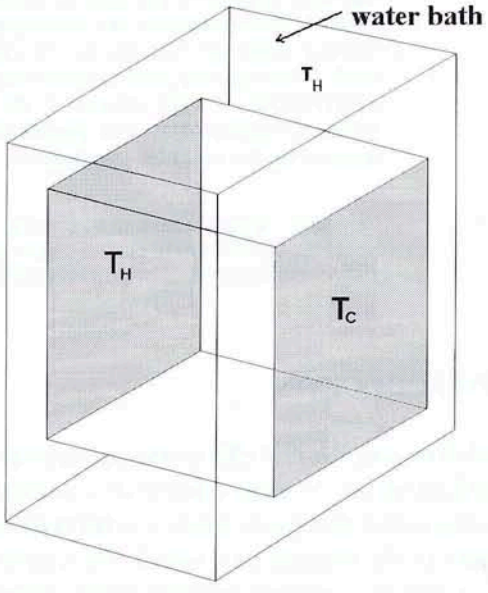

FIGURE 1 The cubical box with differentially heated walls. External water bath (if used) has temperature equal to that of the hot wall (T_h).

initial conditions are investigated. In the first case, we call it here the "cold start" the initial fluid temperature and temperature of all six walls equals $T_o = 0.5°C$, *i.e.*, it is just above the freezing point. The null initial velocity flow field is assumed. The freezing experiment starts, when both hot wall and cold wall temperatures are suddenly changed to $+10°C$ and $-10°C$, respectively. In any physical experiment small temperature fluctuations inside the fluid, non-uniformity of temperature at the external walls, as well as final rise time for the temperature jump, are inevitable. Hence, to improve our definition of the initial condition, the second set of investigations is performed. In this case, we call it the "warm start", the freezing starts after the steady convection pattern is established in the cavity. This initial flow state corresponds to natural convection without phase change in the differentially heated cavity, with the temperature of the cold wall set to $T_c = 0°C$. The freezing experiment starts, when at time $t = 0$, the cold wall temperature suddenly drops to $T_c = -10°C$. In the numerical runs, the solution obtained for steady state natural convection was used as the initial flow and temperature fields to start the freezing calculations.

The three basic dimensionless parameters defining the problem: the Rayleigh number (Ra), the Prandtl number (Pr), and the Stefan number (Ste), are given as

$$\mathrm{Ra} = \frac{g\beta\Delta T H^3}{\alpha\nu}, \quad \mathrm{Pr} = \frac{\nu}{\alpha} \text{ and } \mathrm{Ste} = \frac{c\,\Delta T}{L_f},$$

where $\Delta T = T_h - T_r$ is the temperature difference of the hot wall T_h and the phase interface T_r. In the above definitions g, H, α, β, ν, c, L_f, denote respectively the gravitational acceleration, the cavity height, the thermal diffusivity, the coefficient of thermal expansion, the kinematic viscosity, the specific heat of fluid and the latent heat of fusion.

When variable properties are considered, the non-dimensional description of the problem becomes only formal. Hence, dimensional physical data were used to specify the problem appropriately. For problem description, the non-dimensional parameters defined at the arbitrary selected reference temperature $T_r = 0°C$ were retained. The corresponding non-dimensional values calculated for temperature difference $\Delta T = 10°C$ and 38 mm cavity are: $\mathrm{Ra} = 1.503 \cdot 10^6$, $\mathrm{Pr} = 13.3$ and $\mathrm{Ste} = 0.125$.

Thermal variation of the physical properties of water implemented in the numerical code are given below. The water density function (Fig. 2) was obtained by fitting the fourth order polynomial to the data collected by Kohlrausch (1968) (fit error 0.02%):

$$\begin{aligned}\rho_l = {} & 999.840281167108 + 0.0673268037314653 \cdot t \\ & - 0.00894484552601798 \cdot t^2 + \\ & + 8.78462866500416 \cdot 10^{-5} \cdot t^3 - \\ & - 6.62139792627547 \cdot 10^{-7} \cdot t^4,\end{aligned}$$

where the temperature t is given in degrees Celsius.

The expansion coefficient is obtained by differentiating the above formula:

$$\beta = -\frac{1}{\rho_r}\frac{d\rho}{dT}$$

The remaining relationships for the heat capacity of water, the thermal conductivity and the

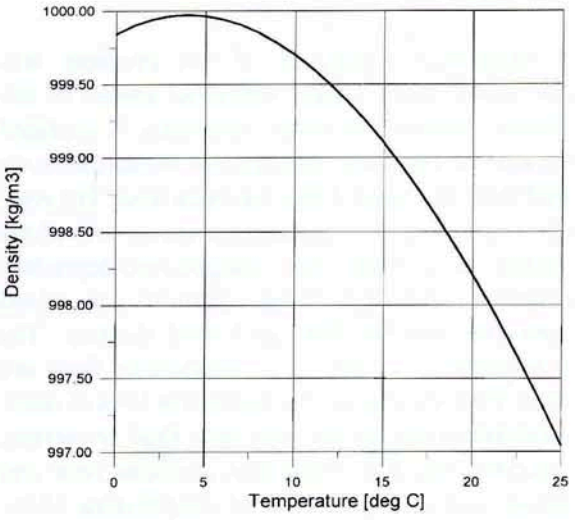

FIGURE 2 Density function of water used in the numerical simulations.

viscosity are those given by Reizes *et al.* (1985) as following functions of the absolute temperature T:

$$c_l = 8.95866 - 0.040534 \cdot T + 1.1234 \cdot 10^{-4} \cdot T^2 - 1.01379 \cdot 10^{-7} \cdot T^3 \,[\mathrm{kJ/kg \cdot K}]$$

$$k_l = 0.566(1 + 0.001 \cdot T)\,[\mathrm{W/m \cdot K}]$$

$$\mu = 1.79 \cdot 10^3 \exp\left[6.18 \cdot 10^7 \left(\frac{1}{T^3} - \frac{1}{(273.15)^3}\right)\right] \times \times [\mathrm{N \cdot s/m^2}]$$

The thermophysical properties of ice were assumed to be constant and equal: $\rho_s = 916.8\,\mathrm{kg/m^3}$ for the density, $k_s = 2.26\,\mathrm{W/mK}$ for the thermal conductivity, and $c_s = 2.116\,\mathrm{kJ/kgK}$ for the heat capacity. The latent heat is equal $L_f = 335\,\mathrm{kJ/kg}$. The thermal conductivity, heat capacity and density of the Plexiglas used were measured. When solving the energy equation for the side walls, the values of $0.195\,\mathrm{W/mK}$ for the thermal conductivity, and $1.19 \cdot 10^{-7}\mathrm{m^2/s}$ for the thermal diffusivity were used. The heat transfer coefficient h used for modelling the convective heat flux from the external fluid was taken to be $1000\,\mathrm{W/m^2K}$ for the forced convection of water and $20\,\mathrm{W/m^2K}$ for the air flow.

NUMERICAL

A numerical simulation of the problem was performed using a finite difference model of the Navier–Stokes and energy equations. A modified version of the three-dimensional numerical code FREEZE3D (Yeoh 1993) has been used. The code allows the study of transient convection with phase change in a fluid with temperature-dependent properties. The governing equations are solved separately for the fluid and solid domain. The governing equations of a Newtonian fluid are those from the physical conservation laws of mass, momentum and energy. The main fluid properties, viscosity, thermal conductivity, specific heat and density are given functions of temperature. However, the density variation is applied in the buoyancy term only.

The vorticity transport equation

$$\frac{\partial \vec{\omega}}{\partial t} + \nabla \times (\vec{\omega} \times \vec{u}) = \mathrm{Pr}[\nabla^2(\mu\vec{\omega}) - \nabla(\vec{\omega}\nabla\mu) + 2\nabla \times (\nabla\vec{u} \cdot \nabla\mu)] + \left[\frac{\mathrm{RaPr}}{\beta_r \Delta_T}\right] \nabla \times \rho\frac{\vec{g}}{g} \quad (1)$$

and energy equation

$$\frac{\partial (c_l\theta)}{\partial t} + \vec{u} \cdot \nabla(c_l\theta) = \nabla \cdot (k_l \nabla\theta) \quad (2)$$

are solved for the fluid domain. The second energy equation is solved in the ice domain

$$\frac{\partial (c_s\theta)}{\partial t} = \frac{\alpha_s}{\alpha_l} \nabla \cdot (k_s \nabla\theta) \quad (3)$$

in which $\vec{u}$, $\vec{\omega}$ are the non-dimensional velocity and vorticity vectors, θ is non-dimensional temperature, α indicates thermal diffusivity, ρ relative liquid density, and subscripts (l, s) are used to indicate physical properties of liquid and solid. To preserve non-dimensional form of the equations all physical properties are given relative to their values at the reference temperature.

For the fluid domain the vorticity-vector potential formulation (Mallinson *et al.*, 1977) is used in the code. The independent variables are vorticity and the vector potential, whereas the pressure is eliminated and the continuity equation is automatically satisfied. As implied by the continuity equation, the velocity vector field is selenoidal. The selenoidal velocity vector field $\vec{u}$ can be represented by another selenoidal vector field:

$$\vec{u} = \nabla \times \vec{\psi}$$

and one obtains the following relationship between the vorticity vector field and the vector potential:

$$\vec{\omega} = -\nabla^2 \vec{\psi} \quad (4)$$

The non-dimensional scaling variables are: the cavity height H for length scale, its ratio with the

kinematic viscosity H^2/v for time scale, and temperature difference $\Delta T = T_h - T_r$ is used to define non-dimensional temperature:

$$\theta = (T - T_r)/\Delta T$$

To couple solutions from both domains, the two fundamental relations must be satisfied at the interface. First, the temperature at the solid–liquid interface is continuous and equal the temperature of fusion: $T_s = T_l = T_r$. Secondly, the energy balance including latent heat released at the interface defines the volume of the solid that is formed. This implies the following condition for normal velocity of the interface:

$$\frac{dn}{dt} = \frac{\mathrm{Ste}}{\mathrm{Pr}} \frac{\rho_l}{\rho_s} \left(\frac{k_s}{k_l} (\nabla \theta_s \cdot \vec{n}) - (\nabla \theta_l \cdot \vec{n}) \right) \quad (5)$$

The Eqs. (1–5) and boundary conditions are solved for a curvilinear coordinate system filling the physical domain. The boundary fitted grid is smoothed using the elliptic grid generation method. As the physical domain changes in shape, the interface boundary grid is generated at each time step. In solving the time dependent partial differential equations, an Alternating Direction Implicit (ADI) method which marches in time is employed. The vector-potential equation is solved using a successive over-relaxation (SOR) method at each time step. A second order central difference approximation for spatial derivatives and a forward difference approximation in time are used.

When simulating experimental conditions, the main problem which arises is the proper definition of thermal boundary conditions (TBC). The two opposite vertical walls and the fluid/solid interface are assumed to be isothermal. The remaining walls are not strictly adiabatic or isothermal. In our study three different approaches were used to test their effect on the final solution. Specifically, the TBC for the non-isothermal walls have been computed using either 1-D or 3-D modelling of the heat flux through/along these walls or idealized adiabatic walls were assumed. In the 1-D TBC approach, so called "convective" TBC were imposed. Using the theory of heat transfer to a thick, infinitely wide plate of uniform conductivity into an external unlimited environment the non-dimensional condition for the temperature θ at the boundary can be written in the general form as:

$$A \cdot \theta + B \frac{\partial \theta}{\partial n} = C \quad (6)$$

The constants A, B and C are calculated from physical properties of fluid/wall material and arbitrary specified heat transfer coefficient assumed in the simulated experiment. By setting A and C equal to zero the adiabatic TBC are obtained.

In the physical situation not only the heat flux through the walls but also along the walls may play an important role. Hence, in the second approach, 3-D TBC case, the additional energy equation for the physical walls has been incorporated into the numerical model, and the coupled fluid–solid heat conduction problem was solved. Then, the simplified boundary conditions obtained from (6) are applied at the external surface of the walls.

Solutions were obtained using 21^3 mesh points for the fluid and $21 \times 21 \times 10$ additional mesh points for the solidus. Using the 3-D TBC five additional grid points were located in each of the four side walls. To test the mesh dependence selected cases were calculated increasing the number of grid points to 31^3 for the fluid domain. To start the freezing calculations the initial grid for the solid phase must exist. Hence, it was assumed that at the first instant the cold wall is already covered with an ice layer of non-dimensional height 0.02.

Flow in a cube is highly three-dimensional. The numerical model used gives us all necessary details about the three-dimensional flow structure. Also the experimental set-up allows us a 3-D reconstruction of the velocity and temperature fields. However, our preliminary numerical and experimental study of 3-D effects suggest their relatively small importance. The interface appears almost

flat across the cavity, and except for small regions in the vicinity of the side walls the velocity and temperature fields can be well approximated by their counterparts observed at the central symmetry plane. Therefore, in the present description we limit our interest to the vertical centre cross-section of the cavity only.

Several cases, covering both the preliminary study of the effect of density anomaly on the fluid flow, as well several different approaches to modelling experimental conditions, were simulated numerically. Table I collects the main parameters used in the performed simulations. The complete collection of the data obtained will be given elsewhere.

To select the most appropriate experimental conditions the preliminary numerical study was performed for the hot wall temperature T_h set to 5°C, 7.5°C, 10°C, 12.5°C and 15°C and adiabatic TBC for the non-isothermal walls. In all cases the cold wall temperature was set to -10°C and the "cold start" initial conditions were used. In this temperature range large variation of the flow pattern and freezing rates were observed, from single counter-clockwise "anomalous" circulation in the lower temperature range, to the similar clockwise "vortex" for the highest temperature (15°C) (comp. Fig. 3). In the middle temperature range, setting 10°C at the hot wall, well defined thermal stratification is present (Fig. 3c). Two main vortices running in opposite directions are separated by the region of density extremum. High velocity and temperature gradients in the region of two colliding flow patterns create challenging conditions for the numerical modelling. Hence, this flow condition was selected for experimental investigations. Analysing Figures 3 it is worth to note the enormous sensitivity of both the flow structure and the freezing front to relatively small changes of the hot wall temperature.

The effect of modelling TBC on the flow structure illustrates Figure 4. Calculations obtained for $T_h = 10$°C have been repeated assuming one dimensional heat flux from the surrounding air (1-D TBC) through the side walls (Fig. 4a), or by including the side walls in the computational domain (3-D TBC – see Figure 4b and Movie 1). It may be seen that the 1-D TBC approach generally

TABLE I Numerical study – initial and boundary conditions

Case	Run	T_H [°C]	TBC*			Heat flux model	Initial conditions**	Main grid	Variable properties
			A	B	C				
External flow – air (plexiglas wall 6 mm) $T_c = -10$°C	#1	+ 5	0	1	0	1-D	cold	21^3	Yes
	#2	+ 7.5	0	1	0	1-D	cold	21^3	Yes
	#3	+ 10	0	1	0	1-D	cold	21^3	Yes
	#4	+ 10	0	1	0	1-D	warm	21^3	Yes
	#5	+ 10	0	1	0	3-D	cold	21^3	Yes
	#6	+ 10	0	1	0	1-D	cold	21^3	No
	#7	+ 10	0	1	0	1-D	cold	31^3	Yes
	#8	+ 10	1	− 1.185	2.5	1-D	cold	21^3	Yes
	#9	+ 10	1	− 0.17	2.5	3-D	cold	21^3	Yes
	#10	+ 10	1	− 0.195	2.5	3-D	warm	21^3	Yes
	#11	+ 12.5	0	1	0	1-D	cold	21^3	Yes
	#12	+ 15	0	1	0	1-D	cold	21^3	Yes
External flow – water (plexiglas wall 9 mm) $T_c = -10$°C	#13	+ 10	1	$-3.04 \cdot 10^{-3}$	1	3-D	warm	21^3	Yes
	#14	+ 10	1	$-3.04 \cdot 10^{-3}$	1	3-D	warm	31^3	Yes

* - the general form of non-dimensional TBC of non-isothermal walls is $A\theta + B(\partial\theta/\partial n) = C$.
** -"cold start": the initial fluid temperature and temperature of all six walls in $T_{in} = 0.5$°C, the null initial velocity flow field is assumed.
"warm start", freezing starts after the steady convection pattern is estavlished in the cavity.

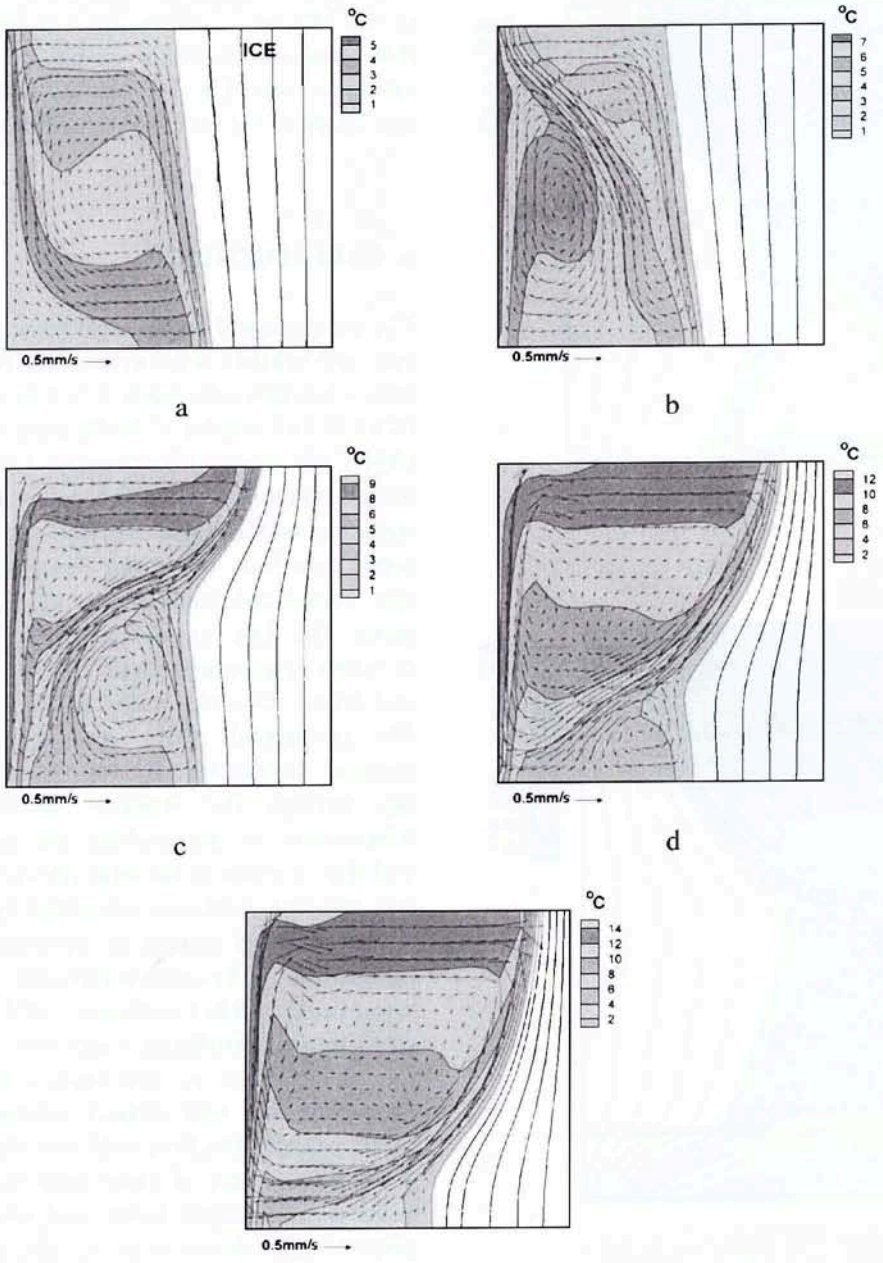

FIGURE 3 Numerical simulation for five freezing regimes at $t = 2500$ s, $T_c = -10°C$, adiabatic TBC and "cold start" in all cases. (a)- run #1, $T_h = 5°C$, Ra = 751528, Ste = 0.0627; (b)- run #2, $T_h = 7.5°C$, Ra = 1127293, Ste = 0.0941; (c)- run #3, $T_h = 10°C$, Ra = 1503057, Ste = 0.1254; (d)- run #11, $T_h = 12.5°C$, Ra = 1878821, Ste = 0.1568; (e)- run #12, $T_h = 15°C$, Ra = 2254586, Ste = 0.1887.

modifies both the flow structure and the temperature field. The most advanced point of the interface moves down and the anti-clockwise circulation becomes smaller. The "improved" 3-D modelling

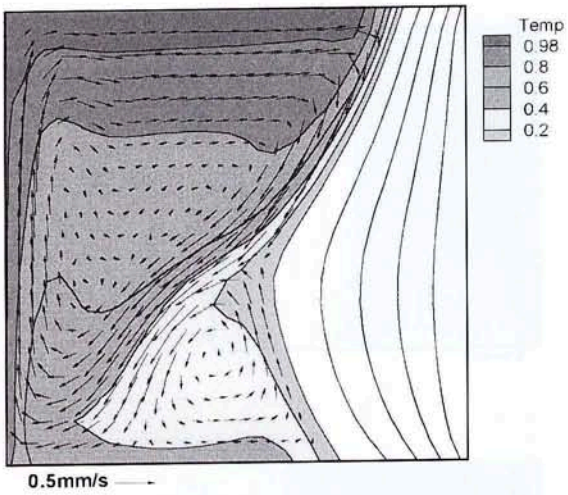

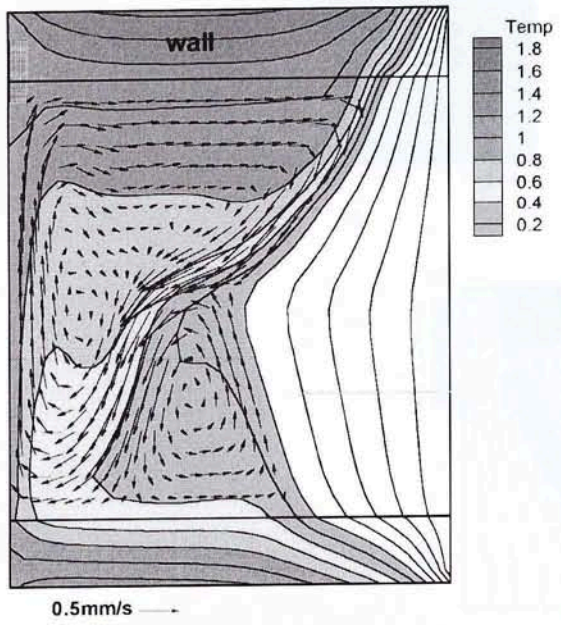

FIGURE 4 Temperature and velocity fields, numerical simulation at $t = 2500$ s for two TBC, $T_c = -10°C$, and "cold start" in both cases. (a)- run #4, 1-D TBC; (b)- run #5, 3-D TBC (for details see Tab. I).

MOVIE 1 Transient development of temperature and velocity fields, ice growing from the right wall. Sequence of numerical results for external fluid air, "cold start", 3-D TBC (run #5); time steps: 60 s, 100 s, 211 s, 300 s, 500 s, 1000 s, 1500 s, 2000 s, 2500 s, 3600 s (corresponds to Fig. 4b). (See Color Plate I at the end of this issue.)

of the TBC has a rather opposite effect. The main flow structure has more similarities to that of the adiabatic case (Fig. 3c), but the temperature field and shape of the interface are different.

3. EXPERIMENTAL

The experimental set-up used to acquire temperature and velocity fields consists of the convection box, a halogen tube lamp, a 3CCD colour camera (KYF55 JVC) and a 32-bit PCI bus frame grabber (AM-CLR Imaging Technology Inc.). The 24-bit colour images of 560×560 pixels were acquired using a 64MB Pentium 133 computer. The convection box, of 38 mm inner dimension, has two isothermal walls made of black anodised metal. The four non-isothermal walls were made of 6 mm (experiments with air as external fluid) and 9 mm (external water bath) thick plexiglas. The isothermal walls were maintained at a constant temperature by anti-freeze coolant flowing through the attached antechamber. The temperature of the cooling and heating liquids and that of water in the bath surrounding the four non-adiabatic walls was controlled by thermostats. The experiment started by opening abruptly the inlet valves to the coolant passages. The temperature of cold and hot wall was $-10°C$ and $+10°C$, respectively. Distillated water was selected as a flow medium for its well known thermophysical properties and well defined temperature of the phase change. The flow field was illuminated with a 2 mm thin sheet of white light from a specially constructed halogen lamp, and observed at the perpendicular direction.

Both velocity and temperature fields were monitored using unencapsulated Thermochromic Liquid Crystal (TLC) tracers (Hiller *et al.*, 1993). The mean diameter of the TLC tracers was about 50 μm. Digital evaluation of tracer images collected for the selected flow cross-section (Digital Particle Image Velocimetry and Thermometry) allows us simultaneous and fully automatic

measurements of temperature and velocity 2-D flow fields. Particle Image Thermometry is based on the temperature-dependent reflectivity of TLCs. If the liquid crystals are illuminated with white light, then the colour of the light they reflect changes from red to blue when the temperature is raised. This occurs within a well defined temperature range (the so-called colour play range), which depends on the type of TLCs used. Temperature is determined by relating the hue (colour) to a temperature calibration function (Kowalewski *et al.*, 1996, 1997), obtained from the images taken for the same fluid, at the same illumination, acquisition and evaluation conditions. Especially developed averaging, smoothing and interpolating techniques are used to remove ambiguity of the resulting isotherms. The 8-bit representation of the hue value assures resolution better than 1%. However, the colour–temperature relationship is strongly non-linear. Hence, the accuracy of the measured temperature depends on the colour (hue) value, and varies from 3% to 10% of the full colour play range. For the TLCs used (TM from Merck) it results in the absolute accuracy of 0.15°C for lower temperatures (red-green colour range) and 0.5°C for higher temperatures (blue colour range). The most sensitive region is the colour transition from red to green and takes place for a temperature variation of less then one degree Celsius. To improve the accuracy of temperature measurements, experiments have been repeated using four different types of TLCs, so that their combined colour play sensitivity range covered temperatures from -5°C to 14°C.

The 2-D velocity vector distribution has been measured by digital particle image velocimetry (DPIV). By this method, the motion of the scattering particles, observed in the plane of the illuminating light sheet, is analysed. For this purpose, the colour images of TLC tracers are transformed to B&W intensity images. After applying special filtering techniques bright images of the tracers, well suited for DPIV, are obtained. Some additional experiments have been performed using colourless "classical" DPIV tracers (*pine pollen* or *lycopodium*).

The magnitude and direction of the velocity vectors are determined using an FFT-based cross-correlation analysis between small sections (interrogation windows) of one pair of images taken at the given time interval. The average particle displacement during a given time interval determines the velocity vector representing the section investigated. Through moving (step by step) the interrogation widow across the image, about 1000 vectors per one pair of images are obtained. The spatial resolution of the method is limited by the minimum number of tracers present in the interrogation window. In practice, the minimum window size was 32×32 pixels. On the other hand, the dimension of the interrogation window limits the maximum detectable displacement. Hence, to improve the accuracy and dynamics of the velocity measurements short sequences of images have been taken at every time step. The cross-correlation analysis performed between different images of the sequence (time interval between pairs changes), allows us to maintain similar accuracy for both the low and high velocity flow regions. The modified multi-quadratic approach was used to interpolate spurious vectors. For some experimental data, the newly developed ODP-PIV method (Quénot *et al.*, 1998) of image analysis has also been used to obtain dense velocity fields of improved accuracy. In the cited paper the results of several accuracy tests performed for flow images generated from a numerical solution are given. It came out that for typical experimental conditions, the accuracy of the "classical" FFT-based DPIV and that of the ODP-PIV method is 0.6 pixels and 0.15 pixels, respectively. It means that for a typical displacement vector of 10 pixels the relative accuracy of the velocity measurement (for single point) is better than 6%.

To get a general view of the flow pattern, several images recorded periodically within a given time interval have been added in the computer memory.

Displayed images are similar to the multiexposed photographs, showing the flow direction and its structure (comp. Fig. 5). This type of visualization is very effective in detecting small re-circulation regions, usually difficult to identify in the velocity field. In all cases studied the volume concentration of tracers was very low (below 0.1%), so their effect on the flow and the physical properties of water was negligibly small.

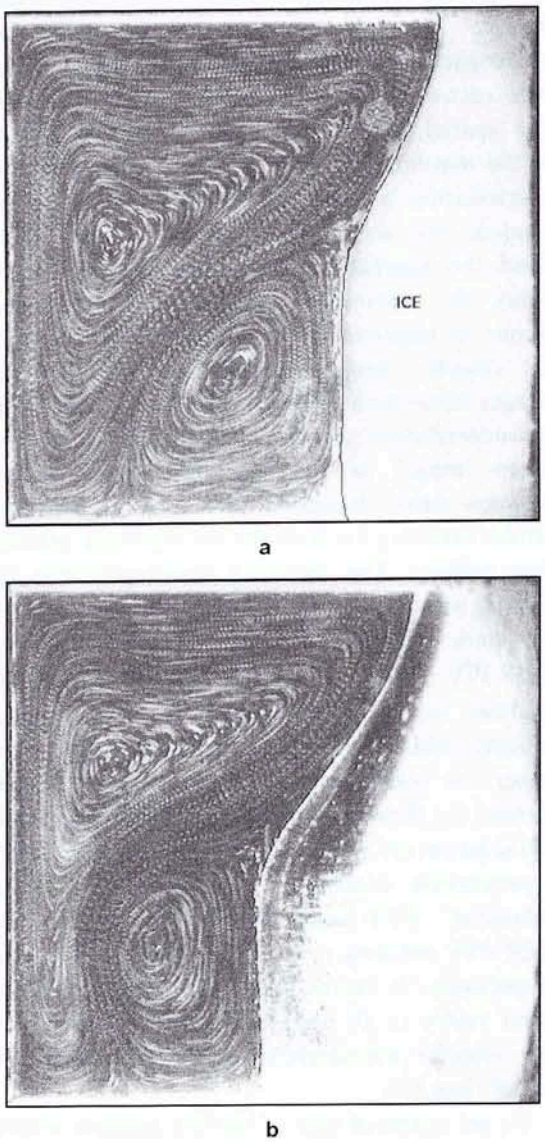

FIGURE 5 Ice fronts observed for the run #1 at 2340 s (a) and 6000 s (b) after cooling starts. Superposition of 10 images taken every 0.4 s.

The flow images are used to evaluate the shape and location of the phase front. These measurements are performed manually using image analysis software. The accuracy of a single points measurement is about 1 pixel, which corresponds to 0.07 mm.

Our main interest was directed to the collection of quantitative information about the phase front position, and the velocity and temperature fields for the centre vertical plane of the cavity. The flow images were collected periodically every 60 s or 120 s, for approximately two hours after cooling was started. The typical set of experimental data consists of 50–60 sequences of four 24-bit images, and uses approximately 250MB disk space.

The main futures of the experiments performed are collected in Table II. Two separate experimental set-ups were employed. In the first configuration the cavity was surrounded by air. The heat transfer from the gas environment through the plexiglas walls is relatively low and its effect on the internal flow was considered to be small. The constant flux of air generated by a low speed fan directed at the cavity was used to make the heat transfer uniform. Both the "cold start" and "warm start" experiments were performed for the cavity surrounded by air. To obtain well defined thermal boundary conditions for the side walls the second configuration was selected. Here, the cavity was immersed in the water bath of constant temperature (forced convection). Only "warm start" initial conditions were possible for that case.

4. SELECTED RESULTS

A large number of experimental data were collected. In the following we have decided to select only a small sample of our results. The detailed collection of a data will be given elsewhere. Selected sets of data are made available for comparisons at our http site.

TABLE II Experimental runs, in all cases $T_c = -10°C$, $T_h = +10°C$

Case	Run	Initial start	Experiment	Tracers
External flow: air 6 mm Plexiglas side walls	#1	"cold"	PIV	Pine
	#2	"cold"	PIV	Pine
	#3	"cold"	PIV + PIT	TLC-B
	#4	"warm"	PIV + PIT	TLC-D
External flow: water 9 mm Plexiglas side walls	#5	"warm"	PIV + PIT	TLC-C
	#6	"warm"	PIV + PIT	TLC-B
	#7	"warm"	PIV + PIT	TLC-D
	#8	"warm"	PIV	Lycopodium
	#9	"warm"	Front location	–

Different experimental runs performed for the same conditions confirmed the reproducibility of the experimental technique. The measured interface profiles and velocity fields from the different runs could be matched within 5–8% error (Fig. 6a). Comparing in this figure interface profiles obtained for two different runs, one may find that the main differences appear at the top of the freezing front for the early time steps. This effect exemplifies the experimental difficulty in matching ideal initial starting flow conditions. The responsible agent is supercooling of water, which delays creation of the first ice layer and deforms the flow pattern at the top of the cavity. Figure 7 and the short movie corresponding to this sequence (Movie 2), demonstrate the problem. Initially, supercooled water at temperature well below freezing point moves along the cold wall to the top of the cavity, sometimes covering even 30% of the upper wall. When suddenly the first nucleation occurs (usually after 30–60 s), the ice front quickly fills this region. The ice layer immobilised at the top quickly melts due to the hot clockwise circulation, but initial disturbance of the flow and temperature fields may affect the front propagation for a longer period.

The experiments performed have shown that the selected case of phase change problem is far from simple and surely worth additional detailed studies. The competing effects of positive and negative buoyancy force, and interacting layers of hot and cold liquid (comp. Fig. 5), create interesting and difficult to model flow patterns. Two main circulations, found in the numerical model, are highly visible: the upper clockwise circulation transporting the hot liquid to the top wall and back along the isotherm of the density extremum, and the lower counter-clockwise circulation within the cold region adjacent to the ice surface. The convective heat transfer between both regions seems to be limited mainly to the upper right corner. There the colliding cold and warm fluid layers intensify the heat transfer and effectively decrease the interface growth. The remaining centre and lower part of the interface is almost parallel to the cold wall, changing its shape very little with time. Here, the freezing process seems to be very little affected by the external convection. The cold water of temperature below 4°C remains trapped in the lower circulation region in the vicinity of the ice interface, which can be easily seen in Figure 8. As the interface moves in time the lower (anti-clockwise) circulation grows (Figs. 8c,d), shifting the diagonal "jet-like" flow into upper parts of the cavity. The position of maximum ice growth coincides with the location where this "jet" separates from the interface. The effect of the initial conditions (comp. Figs. 6a and 6b) is apparent mainly in the early time steps. As the circulation pattern stabilizes, the freezing fronts in both cases readily converge to a similar shape and position.

Interface profiles obtained solving the conjugate thermal problem (3-D TBC) are given in Figure 9. The general behaviour of the ice front is reproduced, but one may see distinct discrepancies between experimental and numerical results. For air as an external fluid the effect of the heat flux

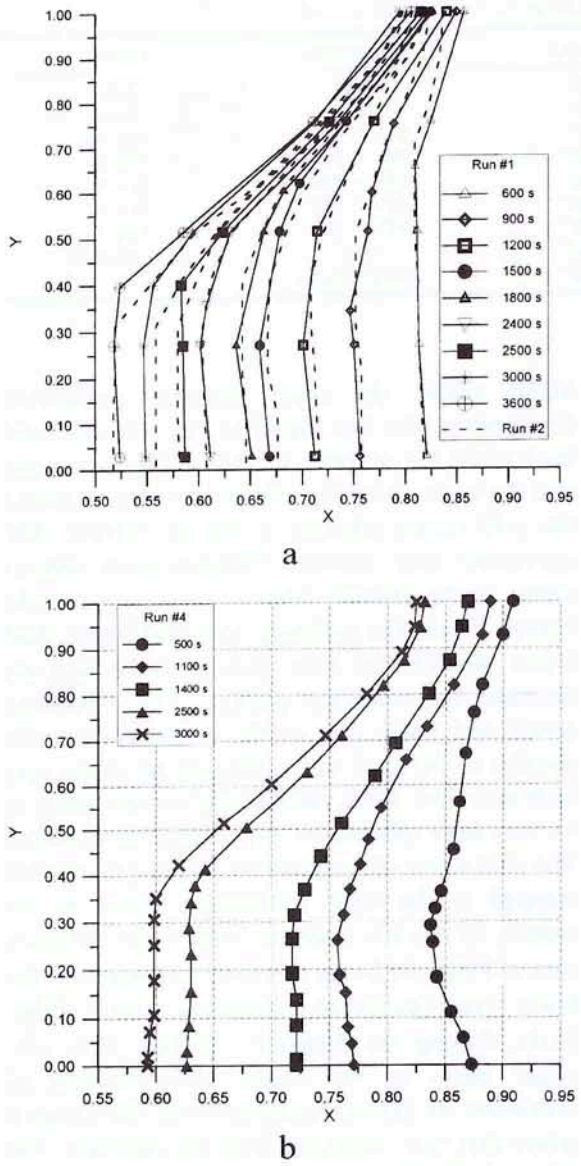

FIGURE 6 Interface profiles measured at selected time steps for the cavity surrounded by air: (a) - run #1, and run #2- "cold start", both runs taken at the same conditions: (b) - run #4, " warm start ".

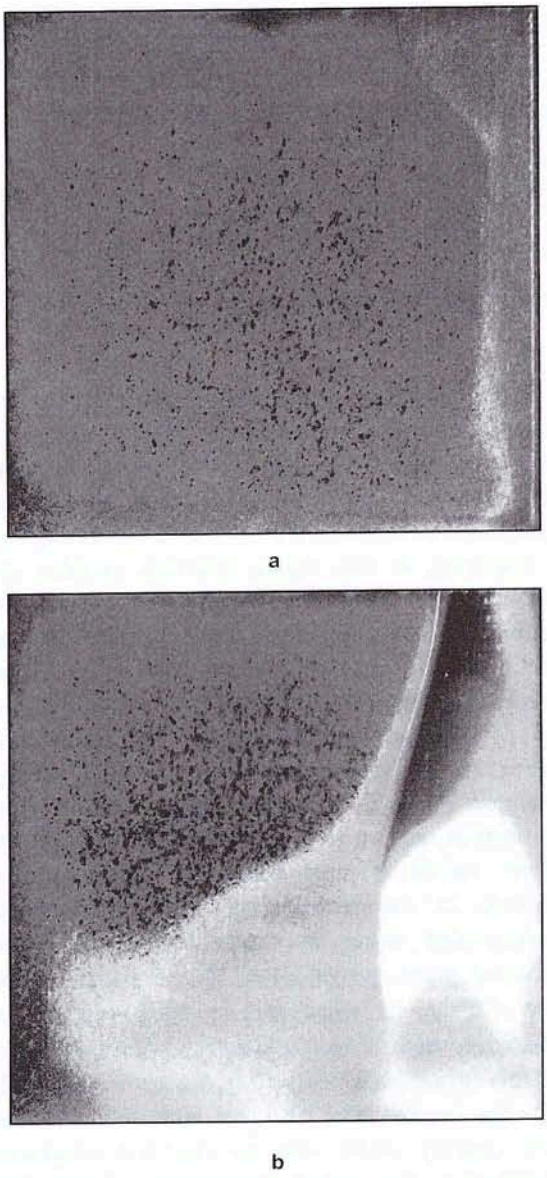

FIGURE 7 Ice front observed for run #7 at two time steps. (a) - 120 s, initial supercooling visible; (b) - 2500 s, well developed circulation. Temperature visualized by TLC tracers, red-green boundary indicates temperature of approximately 4°C.

MOVIE 2 Ice front observed for the run #7 (at right side). Sequence of 60 images taken from beginning of the cooling process to 3000 s. Initial supercooling visible. Temperature visualized by TLC tracers, red-green boundary indicates temperature of approximately 4°C (corresponds to Fig. 7). (See Color Plate II at the end of this issue.)

through the top and bottom walls is small and the experimentally observed contact angle of the ice interface remains almost perpendicular. This is not the case in Figure 9. The effect of heat conduction along the side walls seems to affect the flow structure too strongly. To our surprise, better agreement with the numerical simulation is ob-

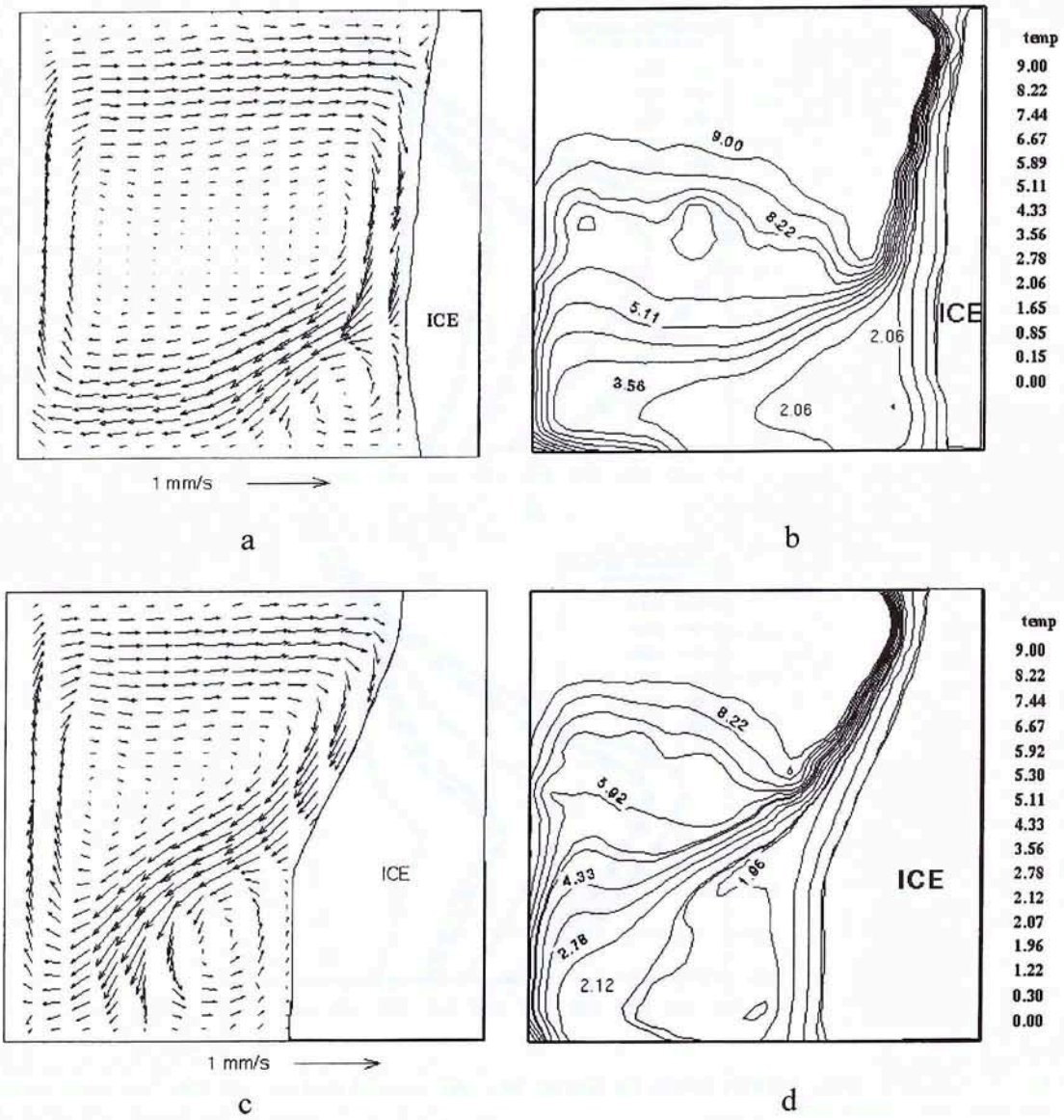

FIGURE 8 Measured velocity and temperature fields at 500 s (a, b) and 3000 s (c, d); run #4: "warm start", external air flow.

tained assuming the idealised adiabatic TBC for the side walls (comp. Figs. 3c and 6).

To elucidate the effect of the side wall conduction, additional experiments were performed (runs #5–#9 in Tab. I), with an external water bath surrounding the convection cavity. The general observation is that the flow pattern is less sensitive than expected to the TBC at the side walls. Even such qualitative change of the external thermal conditions at the side walls hardly modified the freezing rate. Surprisingly, relatively minor changes of ice interface were observed, mainly limited to the bottom region, where additional heat flux through the bottom wall curves the ice

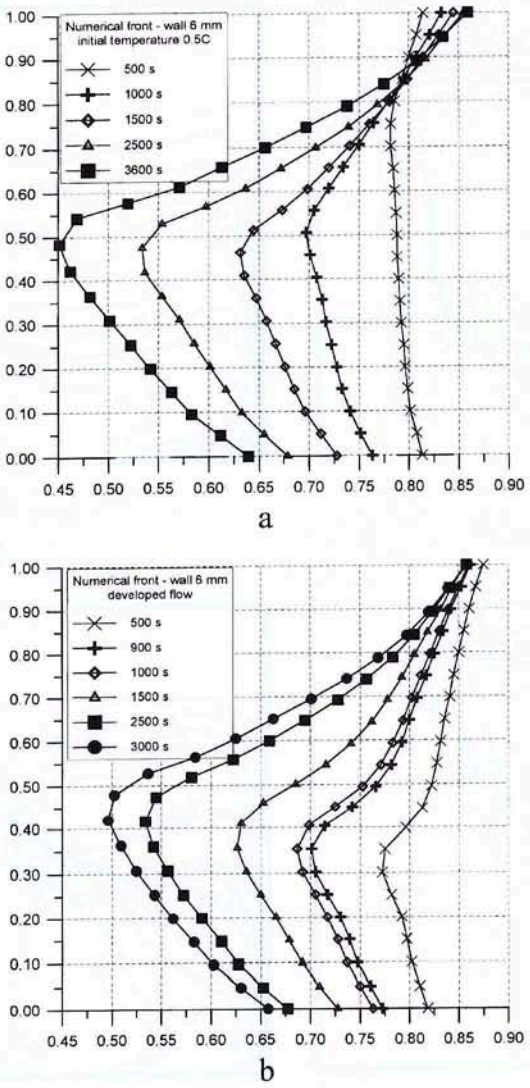

FIGURE 9 Numerical results. Interface profiles for selected time steps, external fluid air, 3-D TBC, two initial conditions. (a) - "cold start" (b) - "warm start".

interface slightly (see Fig. 10). This is not the case in our numerical modelling (Fig. 11). The effect of wall conductivity on the ice interface in the numerical results is again very strong. In comparison with the experiments, the heat flux through the side walls seems to be overestimated (Fig. 12). At the moment we have no simple explanation of this discrepancy.

Selected velocity profiles extracted from the measured flow fields are given in Figure 13. As far as the difference in the front position is small, both measured and calculated velocity profiles match well. The temperature and velocity measurements confirm our general observation that the main fluid circulation takes place in the upper part of the cavity. The fluid temperature there is

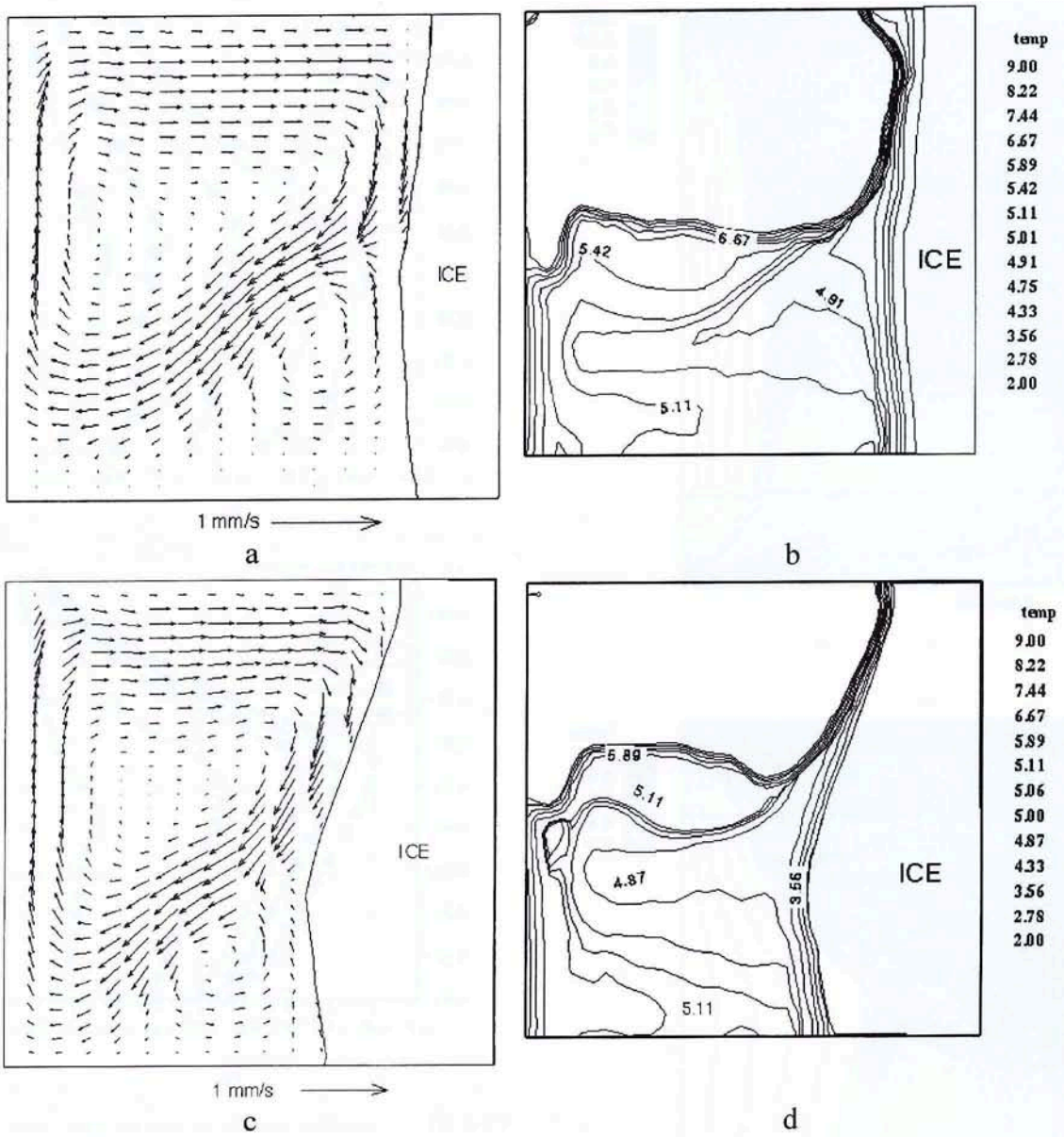

FIGURE 10 Measured velocity and temperature fields at time = 500 s (a, b) and 2600 s (c, d); run #5: "warm start", external water bath.

relatively uniform, close to that of the hot liquid. At the top the average flow velocity is almost one order of magnitude higher then in the bottom region (comp. Fig. 13). Also the largest temperature gradients are present in the lower cavity region. With the progressing ice interface, the lower circulation expands in time on costs of the upper one. This slows down the ice growth, so that even after almost 4 hours of experimental observations less than half of the cavity was frozen.

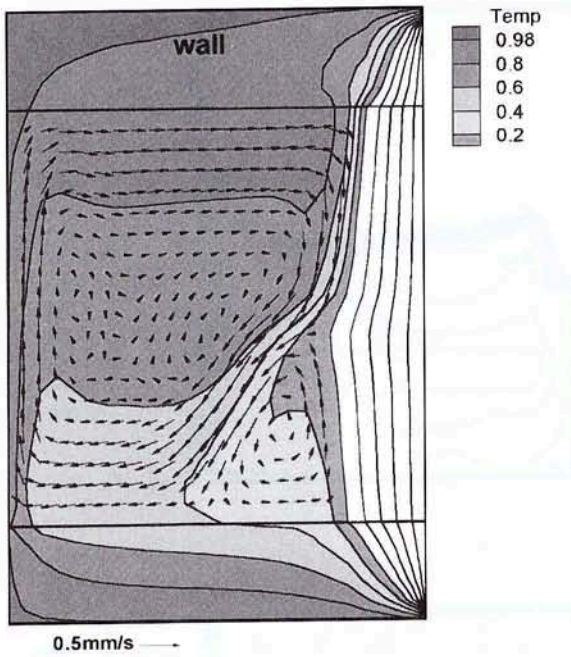

FIGURE 11 Calculated velocity and temperature fields using 3-D TBC, "warm start", external water bath; time step 500s (a) and 2600s (b). (See Color Plate III at the end of this issue.)

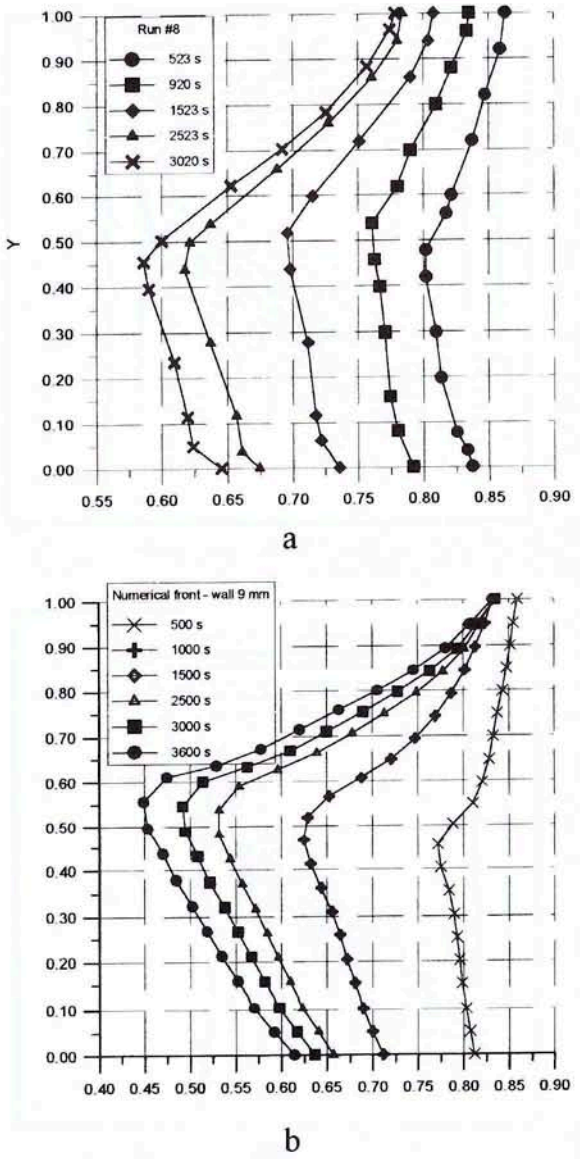

FIGURE 12 Interface profiles at selected time steps, for external fluid water, "warm start"; (a) - measured (run #8), (b) - calculated using 3-D TBC.

5. CONCLUSIONS

The experimental data on freezing of water in the cube-shaped cavity were collected with the purpose of creating a reference for comparison with numerical results. The method of simultaneous

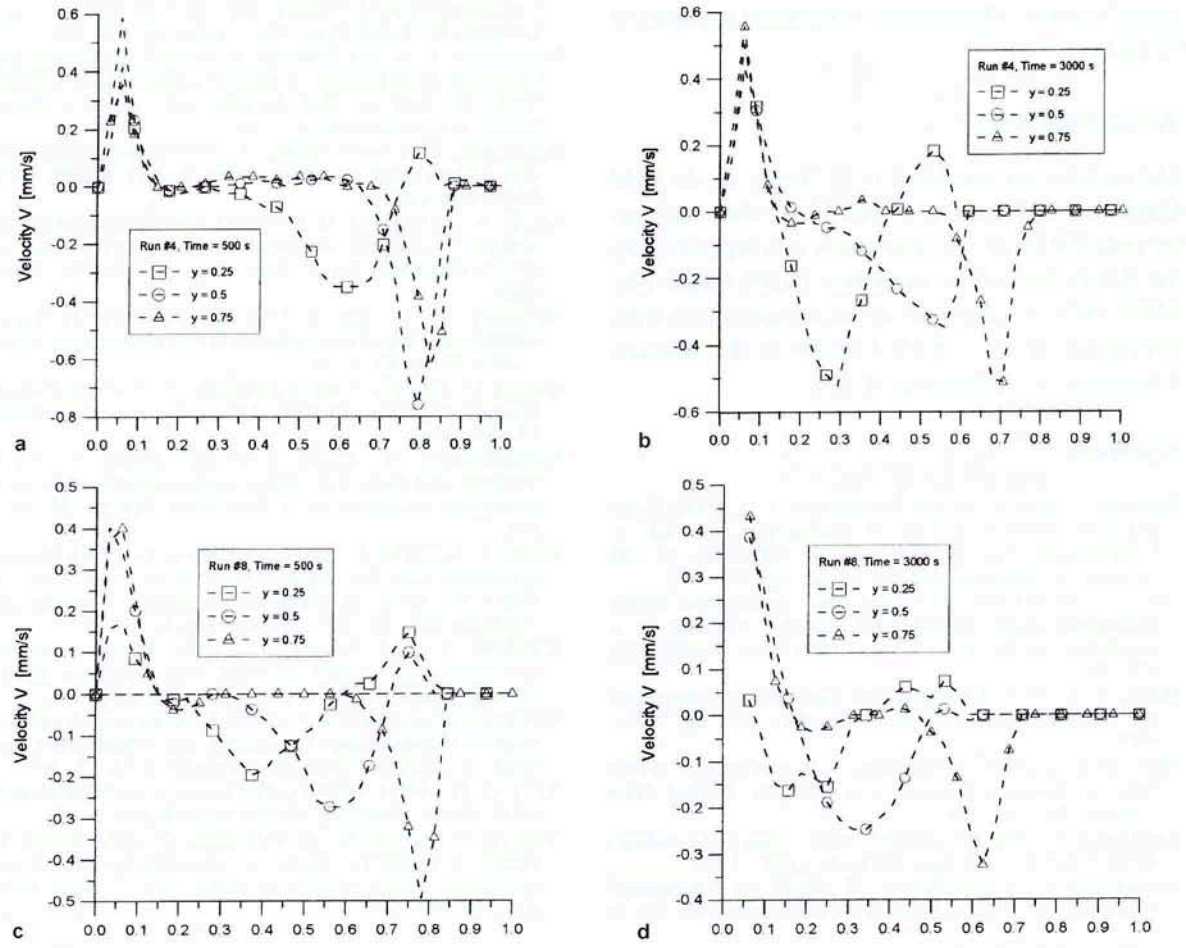

FIGURE 13 Vertical velocity component extracted from PIV measurements. Velocity profiles along cavity taken at relative positions 0.25, 0.5 and 0.75 from the bottom, the "warm start": run #4 (external air) at 500 s (a) and 3000 s (b); run #8 (external water) at time 500 s (c) and 3000 s (d).

measurement of the flow and temperature fields using liquid crystal tracers has been successfully applied to collect transient information on the flow. The collection of results illustrates the complexity of the flow. Its interaction with the ice interface and with the side walls creates two distinct flow regions; the upper adjacent to the hot wall with strong clockwise convection of hot liquid, and the lower region adjacent to the interface with slow counter-clockwise circulation of cold liquid. The mixing of both liquids seems to be small. Hence, the effect of natural convection on the freezing process is mostly limited to the interface near to the top of the cavity. The heat flux through the plexiglas bottom and top walls has relatively little significance for the freezing process. The numerical simulation shows several differences in the front shape and flow pattern. It seems that the model used overestimates the wall conduction. Such effects observed in the experiment as supercooling, stagnant boundary layer at the bottom, imperfections of the ice structure, as well as non-ideal thermal contact between ice and the box surfaces, could be responsible for the discrepancies. Further

numerical and experimental investigations seem to be necessary.

Acknowledgements

The authors are indebted to G. Yeoh, G. de Vahl Davis and E. Leonardi (UNSW) for their computer code FREEZE3D. This work was supported by the Polish Scientific Committee (KBN Grant No. 3T09C00212). Some part of the computations were performed on the CRAY-CS6400 at the Warsaw University of Technology (COI).

References

Banaszek, J., Rebow, M. and Kowalewski, T. A. (1988) Fixed grid finite element analysis of solidification, In: *Adv. in Computational Heat Transfer*, Eds., de Vahl Davis, G. and Leonardi, E., Begell House Inc., Cesme, pp. 471–478.

Gau, C. and Viskanta, R. (1983) Flow visualization during solid-liquid phase change heat transfer: Freezing in a rectangular cavity, *Int. Commun. Heat Mass Transfer*, **10**, 173–181.

Hardy, R. L. (1971) Multiquadratic equations of tomography and other irregular surfaces, *J. Geophys. Res.*, **76**, 1905–1915.

Hiller, W. J., Koch, St., Kowalewski, T. A. and Stella, F. (1993) Onset of natural convection in a cube, *Int. J. Heat Mass Transfer*, **36**, 3251–3263.

Kohlrausch, F. (1968) *Praktische Physik*, Band 3, 22 Auflage, Table 22203, B.G. Teubner Stuttgart, 1.692–1.693.

Kowalewski, T. A. and Rebow, M. (1997) An experimental benchmark for freezing water in the cubic cavity, In: *Adv. in Computational Heat Transfer*, Eds., de Vahl Davis, G. and Leonardi, E., Begell House Inc., Cesme, pp. 149–156.

Kowalewski, T. A. and Cybulski, A. (1996) Experimental and numerical investigations of natural convection in freezing water, *Int. Conf. on Heat Transfer with Change of Phase*, Kielce, *in Mechanics*, **61**/2, 7–16.

Kowalewski, T. A. and Cybulski, A. (1997) Natural convection with phase change (in polish), IPPT Reports **8/1997**, IPPT PAN, Warszawa.

Lin, D. S. and Nansteel, M. W. (1987) Natural convection heat transfer in a square enclosure containing water near its density maximum, *Int. J. Heat Mass Transfer*, **30**, 2319–2329.

Mallinson, G. D. and de Vahl Davis, G. (1977) Three-dimensional natural convection in a box: a numerical study, *J. Fluid Mech.*, **83**, 1–31.

Quénot, G., Pakleza, J. and Kowalewski, T. A. (1998) Particle Image Velocimetry with Optical Flow, *Experiments in Fluids*, **25**, 177–189.

Ramachandran, N., Gupta, J. P. and Jaluria, Y. (1982) Thermal and fluid flow effects during solidification in a rectangular enclosure, *Int. J. Heat Mass Transfer*, **25**, 187–194.

Reizes, J., Leonardi, E. and de Vahl Davis, G. (1985) Natural convection near the density extremum of water, *Proc. of Fourth Int. Conf. on Numerical Methods in Laminar and Turbulent Flow*, pp. 794–804, Swansea, U.K.

Robillard, L. and Vasseur, P. (1981) Transient natural convection heat transfer of water with maximum density effect and supercooling, *Trans. ASME*, **103**, 528–534.

Viswanath, R. and Jaluria, Y. (1993) A comparison of different solution methodologies for melting and solidification problems in enclosures, *Num. Heat Transfer B*, **24**, 77–105.

Yeoh, G. H. (1993) Natural convection in a solidifying liquid, *Ph.D. Thesis*, University of New South Wales.

Yeoh, G. H., Behnia, M., de Vahl Davis, G. and Leonardi, E. (1990) A numerical study of three-dimensional natural convection during freezing of water, *Int. J. Num. Meth. Eng.*, **30**, 899–914.

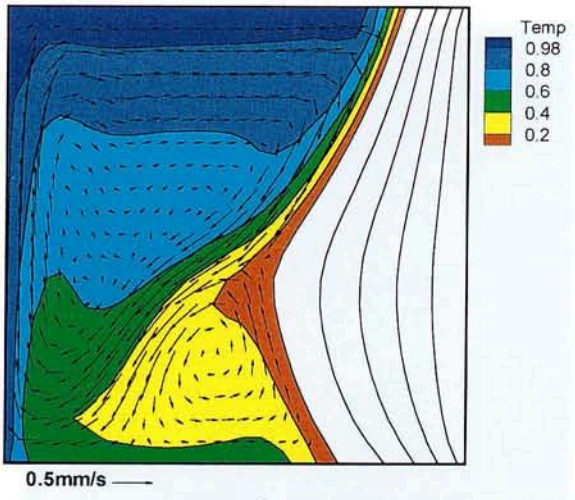

a

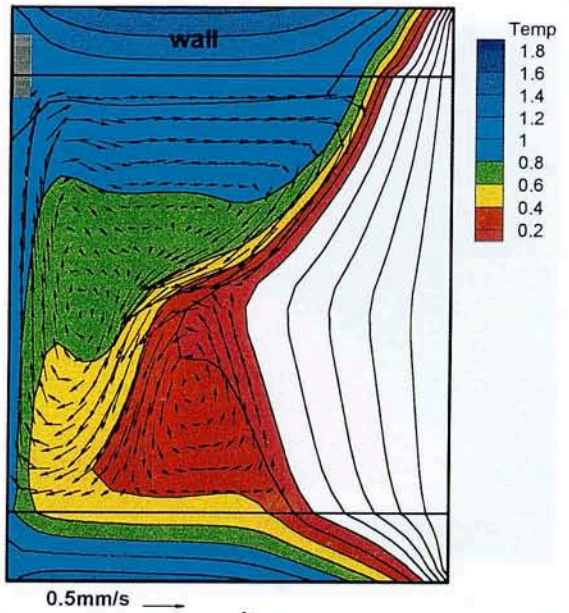

b

COLOR PLATE I (See T. A. Kowalewski and M. Rebow, page 200).

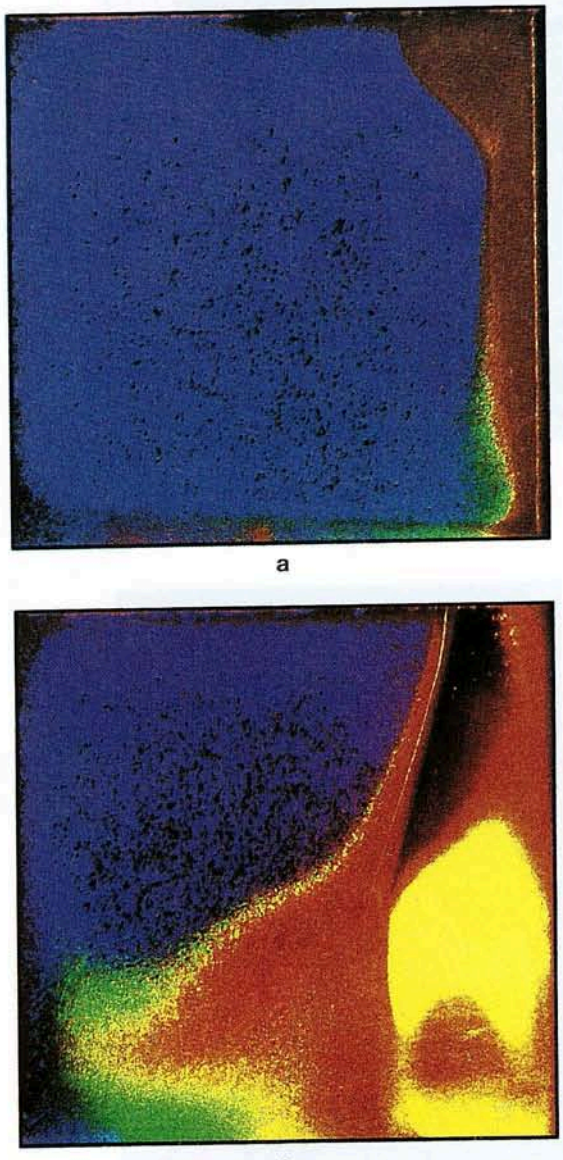

a

b

COLOR PLATE II (See T. A. Kowalewski and M. Rebow, page 204).

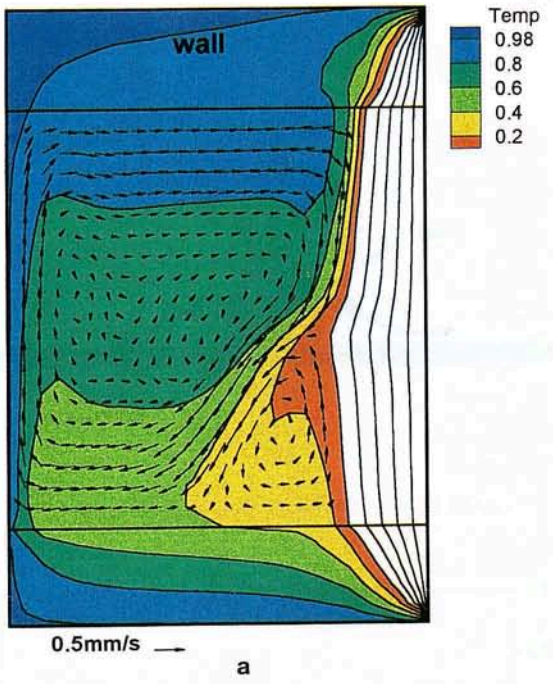

a

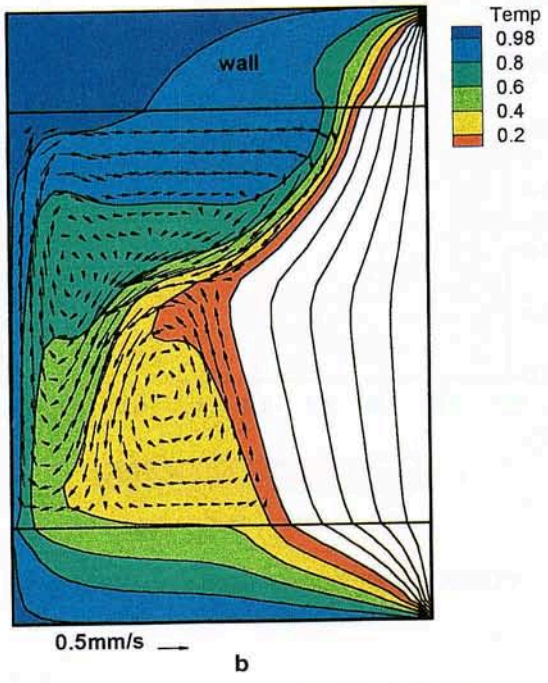

b

COLOR PLATE III (See T. A. Kowalewski and M. Rebow, page 208).